NASA CR-132358

ANALYSIS OF THE FLOW ABOUT DELTA WINGS WITH LEADING EDGE SEPARATION AT SUPERSONIC SPEEDS

By Joseph P. Nenni and Chee Tung

Prepared Under
Contract No. NAS1-11577
Calspan Corporation
Buffalo, New York 14221

for

NATIONAL AERONAUTICS AND SPACE ADMINISTRATION

ANALYSIS OF THE FLOW ABOUT DELTA WINGS WITH LEADING EDGE SEPARATION AT SUPERSONIC SPEEDS

By Joseph P. Nenni and Chee Tung
Calspan Corporation

I. SUMMARY

A research program was conducted to develop an improved theoretical flow model for the flow about sharp edge delta wings with leading-edge separation at supersonic speeds. The flow model incorporates a representation of the secondary separation region which occurs just inboard of the leading edge on such wings and is based on a slender-wing theory whereby the full three-dimensional problem is reduced to a quasi two-dimensional problem in the cross-flow plane.

The secondary separation region was modeled by a surface distribution of singularities or a linearized type of cavity representation. The primary vortex and separation were modeled by a concentrated vortex and cut in the cross-flow potential which represents its feeding sheet (in the sense of Brown and Michael). The formulation is made determinate by requiring that the stream lines in the cavity region be conical rays, by imposing a cavity closure condition, by applying a Kutta condition at the wing leading edge, and by requiring that the primary vortex and its feeding sheet be force free. The flow model reduces to that of Brown and Michael in the limit of zero cavity width.

The cross-flow solutions for the cavity model were obtained, but these solutions have physical significance only in a very restricted range of angle of attack. The reasons for the failure of the flow model are discussed. The analysis is presented so that other interested researchers may critically review the work.

The second order corrections to slender-wing theory for this flow model, for nonslenderness and compressibility, have been formally derived using matched asymptotic expansions. In the limit of zero cavity width, these results reduce to the second-order-theory previously obtained by the authors using the Brown and Michael cross-flow model. In this case certain improvements have been implemented in the method of obtaining the surface pressure distributions from the velocity potential. The agreement between theory and experiment is thereby improved over a limited Mach number range.

II. INTRODUCTION

The flow field about low aspect ratio or slender wings that exhibit leading-edge separation has been of concern to designers of high-speed aircraft and lifting reentry vehicles for some time. The unique features

of such flow fields are the spiral sheets of vorticity that emanate from highly swept leading edges and dominate the flow field on the lee side of the wing or vehicle. This separation produces a nonlinear aerodynamic behavior of the wing as angle of attack is varied.

Although the main features of these flow fields have been recognized for almost twenty years, no completely satisfactory theoretical analysis has been developed. Polhamus (Reference 1) has developed an accurate analytical method utilizing an intuitive leading-edge suction analogy for estimating overall forces on slender wings. However methods to predict detailed flow quantities such as surface pressures and loadings are needed. Moreover, a further understanding of such vortex flows would aid in the design of optimum wings for supersonic flight and open up the possibilities for control of the flow over such wings.

The problem is fundamentally non-linear through the boundary conditions because the location of the spiral vortex sheets is unknown a priori. However, for compressible flow the exact equations of motion are also non-linear. Existing analyses for the detailed flow quantities have used slender-wing theory whereby the problem is reduced to a quasi two-dimensional incompressible problem in the cross-flow plane. The nonlinearity in the boundary conditions may then be handled by the use of complex variable theory in the cross-flow plane. The most notable efforts in this vein were made by Brown and Michael (Reference 2), Mangler and Smith (Reference 3), and Smith (Reference 4). These analyses differ only in the representation of the spiral sheet in the cross-flow plane. Brown and Michael use a concentrated vortex connected to its corresponding leading edge by a cut in the cross flow velocity potential. Mangler and Smith used a more realistic spiral representation of the vortex sheet terminated by a cut and concentrated vortex in the core area of the spiral sheets. Smith refined this representation still further by essentially considering more wraps of spiral sheet. A refined representation of the core area has been considered by Mangler and Weber (Reference 5).

Comparison between theory and experiment shows that the existing slender-wing theories greatly overestimate the forces on low apsect ratio wings. (For example, the slender wing result is high by almost a factor of two in the moderate angle of attack range.) The possible reasons for this discrepancy have been attributed to an inadequate cross-flow model and the neglect of higher order aspect ratio and Mach number terms in the equations of motion.

A second order theory was developed by the present authors, in Reference 6, to account for non-slenderness and compressibility effects. The Brown and Michael cross-flow model was used for ease of analysis since the gross predictions of this model were similar to those of References 3 and 4. The consideration of these corrections improved the correlation between theory and experiment, but did not remove all discrepancies. It was, however, clear from the results of Reference 6 that, in terms of total lift on the wing, compressibility and nonslenderness effects were more important than refinements in the representation of the primary separation and vortex sheet. The essential fault with either flow models of Reference 2 and 3 is that the

predicted vortex positions are close to the wing surface, which results in overprediction of the upper surface suction pressures. It may be concluded that a fundamental change in the cross-flow model is required to improve the prediction of vortex location and strength. In short, it was felt that neither cross-flow model incorporated all of the features that may be physically significant to the flow field.

The major features of the cross-flow as observed from flow-field and surface-flow studies (see for example, References 7, 8, and 9) are shown sketched in Figure 1. The details of the secondary separation region have not been thoroughly explored. In some instances additional flow separations and reattachments may be observed close to the upper surface leading edge; however, further categorization of this flow region does not appear to be warranted at this time. All of these major features except the secondary separation region have been considered to some degree of approximation in the previous analysis. Hence, it was suspicioned that the secondary separation region must be modeled to resolve the discrepancies between theory and experiment. Moreover, although the secondary separation occurs only over a minor portion of the wing span, it can have important effects upon the manner in which the flow leaves the wing surface and forms the primary spiral vortex sheets.

A rational, but unsuccessful, attempt to include secondary separation in the cross flow model is described in this report. The secondary separation was modeled by a surface distribution of singularities and the primary separation in the Brown and Michael sense. In effect the separation is modeled as a cavity and in the limit of zero cavity width the flow model reduces to that of Reference 2. Unfortunately the mathematical solutions for this flow model have physical significance only in a limited angle of attack range near zero angle of attack. The reasons for the failure of this model are discussed and the results are presented to allow other interested researchers to review the analysis critically.

The cavity flow model was formally incorporated into the previously developed second-order theory and in the limit of zero cavity width this theory reduces to the results of Reference 6.

In Reference 6 the surface pressure distributions were obtained from the velocity potential by using an approximate form of the isentropic pressure-velocity relationship obtained by series expansion. In unpublished calculations this expression was found to give spurious results at high Mach numbers. The series expansion employed was not valid for high Mach numbers. This shortcoming of the previous theory has been partially overcome by using the exact isentropic pressure-velocity relationship to calculate surface pressures from the velocity potential. This can only be accomplished for limited Mach number and angle of attack ranges because, at sufficiently high Mach numbers and/or angles of attack, the theory predicts surface velocities which exceed vacuum conditions. (This is also a consequence of the vorticies being too close to the wing.) In this limited range, however, the correlation between theory and experiment is improved. This work is described in Section IV of the report.

III. LIST OF SYMBOLS

a - ratio of wing span to root chord

AR - aspect ratio

c - cavity width in x plane

C_L - lift coefficient

C_N - normal force coefficient

C_p - pressure coefficient

$C_{p\,vac}$ - pressure coefficient at vacuum conditions

$f(n)$ - source strength in cavity region

$G_1(s)$ - portion of solution for $\bar{\Phi}_{11}^{\prime}$

h - normalized half span of wing (it is a function of x and is sometimes written as $h(x)$ to emphasize this dependency)

H - function defined in Equation 8

H_3 - function defined by Equation 22

H_4 - function defined by Equation 24

i - $\sqrt{-1}$

I.P. - imaginary part of complex function

M_∞ - free-stream Mach number

p - real coordinate of vortex core in physical plane

$\bar{P}(s)$ - line doublet strength for outer solution

q - imaginary coordinate of vortex core in physical plane

$Q(s)$ - line source strength for outer solution

r - distance from S axis in $S, \underline{\eta}, \zeta$ space ($r = \sqrt{\underline{\eta}^2 + \zeta^2}$)

R_e - Reynolds number based on root chord

R.P. - real part of imaginary function

$S, \underline{\eta}, \zeta$ - strained outer variables

S, Y, Z - strained inner variables

T - normalized cavity thickness

U_∞ - free stream velocity

W_{11} - complex potential for first inner solution

W_{121} - complex potential for second inner solution

x, y, z - Cartesian coordinates normalized by one-half the root chord

α - angle of attack

β - $\sqrt{M^2 - 1}$

γ - normalized vortex strength (Γ / h)

Γ - vortex strength

δ - parameter defined in Equation 7

$\bar{\gamma}$ - ratio of specific heats

$\bar{\epsilon}$ - angle of attack parameter ($\sin \alpha / \tan \Lambda$)

λ - real coordinate of vortex in χ plane

λ_c - inboard edge of cavity in physical plane

ξ_1 - straining of χ coordinate

σ - complex inner variable, $z + iy$

σ_1 - position of vortex in σ plane

Λ - delta wing semi-apex angle

η - imaginary part of χ

τ - imaginary coordinate of vortex in χ plane

Φ - velocity potential

$\bar{\Phi}^{\lambda}_{11}, \bar{\Phi}^{\lambda}_{121}, \bar{\Phi}^{\lambda}_{122}$ - inner solution for velocity potential

χ - complex transformation of σ plane

χ_1 - position of vortex in χ plane

ψ_1, ψ_2 - decomposition of λ

IV. OUTLINE OF MATHEMATICAL FORMULATION

The general perturbation method presented in Reference 6 for determining the velocity potential is employed again and will only be outlined briefly.

The coordinate system used is shown in Figure 2. This system is a body axis system and the wing leading edge is given by $z_{l.e.} = a\,h(x)$. The physical spatial variables are normalized by one-half the root chord such that the wing apex is located at $x = -1$ and the trailing edge at $x = +1$. Then, for a delta wing, $h = \frac{1}{2}(1+x)$.

For infinitely thin wings the velocity potential is expanded as

$$\Phi \sim U_\infty \left\{ x\cos\alpha + \sin\alpha\,\psi_1 + \sin^2\alpha\,\psi_2 \right\}$$

and the independent spatial variables may be strained in the typical P.L.K. fashion as (see Reference 6)

$$y = \underline{\eta}$$

$$z = \zeta$$

$$x = S + \xi_1 \sin\alpha$$

The straining in the axial direction, ξ_1, is determined by the principle that "the higher order solutions shall be no more singular than the first order solution." This expansion procedure decomposes the original nonlinear problem into a sequence of linear poblems. The governing partial differential equations and boundary conditions on the ψ_i are given by Equations 7, 10, 12, and 15 in Reference 6.

For wings of small aspect ratio the ψ_i are determined by the method of matched asymptotic expansions. The small parameter used is a, the ratio of wing span to root chord. The outer expansion for ψ_1 valid far from the wing and for small a is of the form

$$\psi_1^o \sim \underline{\eta} + a\,\phi^o_{11_J} + a^2\phi^o_{11_D} + o(a^4) \tag{1}$$

where $\phi^o_{11} = \Phi^o_{11}(\eta,\zeta,S)$ and $\phi^o_{11_J}$ is the potential for a line source distribution and $\phi^o_{11_D}$ is the potential for a line doublet distribution. The doublet distribution is required for lifting flows and the source distribution is required because the cavity representation for the secondary separation region effectively gives the wing thickness. The appropriate forms are

$$\phi^o_{11_J} = -\frac{1}{2\pi}\int_{-1}^{S-\beta r} \frac{Q(S_o)\,dS_o}{\left[(S-S_o)^2 - \beta^2 r^2\right]^{1/2}} \tag{2}$$

$$\phi^o_{11_D} = \frac{1}{4\pi}\frac{\eta}{r}\int_{-1}^{S-\beta r} \frac{\bar{P}(S_o)(S-S_o)\,dS_o}{\left[(S-S_o) - \beta^2 r\right]^{1/2}} \tag{3}$$

where

$$r^2 = \eta^2 + \zeta^2$$

$$\beta^2 = M_\infty^2 - 1$$

The source strength $Q(S_0)$ and the doublet strength $\bar{P}(S_0)$ will be determined later by the matching conditions between inner and outer solutions. The inner problem is obtained by stretching the coordinates normal to the wing to regain the detail lost near the wing. The inner variables are

$$Y = \eta/a$$

$$Z = \zeta/a$$

$$S = S$$

Then the inner solution valid near the wing for small values of a is of the form

$$\psi_i \sim a\,\Phi_{i1}(Y,Z;S) + a^3\Phi_{i21}(Y,Z;S) + a^3 \ln a\,\Phi_{i22}(Y,Z;S) + O(a^4, a^4 \ln a) \tag{4}$$

The partial differential equations for the Φ^i are given by Equations 26, 27, and 28 of Reference 6. The important point to note is that these equations are two dimensional in Y and Z with S appearing only as a parameter. The first inner solution Φ_{i1} satisfies LaPlace's equation in the plane transverse to the wing and the appropriate form of surface flow tangency. This first inner solution is the standard "cross-flow problem" of slender-wing theory and may be solved by conformal mapping techniques of complex variable theory. The first inner solution may be expressed as

$$\Phi_{i1} = R.P.\,W_{i1}(\sigma) + G_i(S)$$

where σ is the complex variable $Z + iY$ and W_{i1} is referred to as the complex velocity potential. The $G_i(S)$ term is required because of the source-like behavior of the cavity, and it is determined by matching with an outer solution.

A brief review of the experimental observation of the cross-flow and the detailed formulation of the cross-flow model used is presented in the next section.

V. THE CROSS-FLOW MODEL

Review of Experimental Observations of the Cross Flow

The tentative concept of the actual cross-flow model for slender wings is shown in Figure 1, deduced largely from the vapor screen studies of References 7 and 10, the smoke flow studies of References 8 and 11, and the surface flow studies of References 13 and 14. (These references have been selected because of the quality of the photographic material contained in them rather than on

chronological order or originality.) These flow features are present regardless of the Mach number as long as the leading edge is subsonic.

There are some systematic differences evident in the cross-flow model at subsonic and supersonic speeds. The vapor screen studies of Reference 8 indicate that at supersonic speeds the vortex pattern is spread over a greater spanwise extent of the wing and lies closer to the wing surface than at subsonic speeds. Comparison of surface pressure distributions (as between References 10 and 12) also confirms the observation that the vortex pattern is more diffused at supersonic speeds.

Details of the secondary separation region are dependent upon Reynolds number. The spanwise flow evidently separates because it cannot negotiate the pressure rise between the negative pressure peak (underneath the vortex core) and the leading edge. Available experimental data indicate that the primary Reynolds number effect is through boundary layer transition and its proximity to the secondary separation line. There is some experimental evidence which indicates that for the higher aspect-ratios, reattachment occurs between the secondary separation region and the leading edge.

An example of Reynolds number effects on the surface pressure distributions may be seen in Figure 3 which shows some subsonic data from Reference 11. As Reynolds number increases, the magnitude of the upper surface pressure peak increases, and the lateral extent of the vortex pattern decreases. Apparently, after the boundary layer at the secondary separation point becomes fully turbulent, the Reynolds number dependence becomes very weak. The spanwise pressure distributions also indicate that at the lower Reynolds numbers the secondary separation region contains several discrete longitudinal vortices (as indicated by the variations in pressure) while at higher Reynolds numbers the secondary separation is more like a cavity (as indicated by the uniformity of the pressure). Although the pressure distributions are markedly affected by Reynolds number, the normal force and pitching moment are independent of Reynolds number. (The wing root bending moments which have not been measured, however, must be affected.)

It must, however, be concluded that the existence of any secondary separation region is a significant factor in the observed differences between theoretical predicted forces and experimentally determined forces. Since the theoretical values are higher, the foregoing discussion would indicate that the secondary separation region of slender wings is an area where boundary layer control devices may be used to increase the lift on such wings. Complete elimination of the secondary separation region should move the experimental results closer to the theoretical results.

The experimental investigations of Reference 14 indicate that at transonic speeds there are similar effects of Reynolds number on the pressure distribution. However, at transonic speeds the normal force and pitching moments are also dependent on Reynolds number. These results cast some doubt as to whether the existing supersonic data are free of Reynolds number effects. More experimental work is needed in the supersonic speed regime to investigate

Reynolds number effects. Moreover, additional detailed flow field and surface pressure measurements near the leading edge are needed to investigate the character of the secondary separation region.

Mathematical Flow Model

The secondary separation region is properly modeled by a volume distribution of singularities over the separation region. However, since this representation is mathematically intractable at present, a simpler representation was sought. Since the height of the secondary separation is small compared to the other wing or flow field dimensions, it appeared permissible to collapse the volume singularity distribution to a surface singularity distribution. Indeed, inspection of the vapor screen studies of Reference 7 would suggest that at low angles of attack even the primary separation might also be modeled by a surface singularity distribution. (This type of flow model was considered further and will be discussed later in Appendix A.) Such a flow model would then be generically related to that used in Reference 15 to analyze the flow over a partially cavitated, low-aspect-ratio hydrofoil. Hence, the terminology of cavity has been used for this surface singularity distribution. For reasons discussed previously the Brown and Michael representation of the primary separation was considered adequate for present purposes.

Inclusion of the secondary separation in the flow model requires the development of additional boundary conditions to make the problem determinate. Since the condition of flow tangency at the wing surface must be abandoned in the cavity region, one of the other flow quantities must be prescribed on the cavity. In the hydrofoil case, Reference 15, the pressure is specified as constant along the cavity, but this is not appropriate for aerodynamic problems. The required constraint for the present flow model was deduced from inspection of surface flow patterns, primarily those shown in Reference 9. Inspection of these photos shows that in the secondary separation region the surface streamlines are conical rays emanating from the wing apex and this was the condition used, being equivalent to making the transverse velocity parallel to the wing in the cross flow plane equal to $v_\infty z/s$. Since the wing surface in the cross-flow plane also has a transverse velocity of $v_\infty z/s$, this condition implies that in the cavity region of the cross-flow plane there is no relative transverse velocity between the flow and the wing. Then, according to the definitions of separation in three-dimensional flow given by Maskell in Reference 16, the inboard edge of the cavity is automatically a separation line. In total, then, the conical streamline requirement in the cavity region appears to be consistent with all of the physical requirements for modeling the secondary separation region.

One additional constraint is required to make the problem determinate. The condition selected was that of cavity closure. To the inviscid flow outside the cavity, the cavity appears as a local thickening of the wing. The cavity closure condition is then the requirement that the cavity has no thickness at its edges, implying that the flow that leaves the wing surface

at the inboard edge of the cavity reattaches to the wing at the leading edge before departing from the wing surface and becoming entrained in the primary separation flow pattern.

The resulting cross-flow model and applicable boundary value on the velocity potential are shown in Figure 4. The subscript notation has been used to indicate partial differentiation with respect to the appropriate variable. The concentrated vortices are located at σ_1 and $-\bar{\sigma}_1$ and are connected to their respective leading edges by a cut in the cross-flow potential. The cut then represents a planar vortex sheet in the three-dimensional flow with the axis of the vorticity vector in the cross-flow plane. In this fashion the cuts serve as the feeding sheets for the concentrated vortices. The cavity extends between λ_c and h .

This boundary value problem is most easily handled by using conformal transformations. The transformation chosen was

$$\chi = \sqrt{\sigma^2 - h^2} \tag{5}$$

The branches of the square root are chosen such that the upper wing surface is mapped into a line segment along the positive imaginary axis and the lower wing surface is mapped into a line segment along the negative imaginary axis. The flow in the χ plane is shown in Figure 5. Any analytic function with the proper symmetry in this plane automatically satisfies the condition of no flow through the wing. The cavity is represented by a source distribution in this plane that extends between the origin and ic. The vortices are mapped to χ_1 and $-\bar{\chi}_1$. The appropriate complex potential is then given by

$$W_{11}(\chi) = -i\chi + \int_0^c f(\eta_0) \ln(\chi - i\eta_0)\, d\eta_0 - i\frac{\Gamma}{2\pi}\left[\ln(\chi - \chi_1) - \ln(\chi + \bar{\chi}_1)\right] \tag{6}$$

Whereas the first term gives the flow about the wing without any additional singularities in the flow field, the second term gives the flow due to a distribution of sources of local strength $f(\eta_0)$ along the cavity, and the last term gives the flow due to the concentrated vortices . The source strength is given by the requirement for conical streamlines in the cavity area. In terms of the velocity potential this is

$$\begin{aligned} \Phi^i_{11_Z} &= \delta Z \qquad \text{on } Y = 0, \quad \lambda_c \le Z \le h \\ \delta &= -\frac{1}{\epsilon h} \end{aligned} \tag{7}$$

Utilizing the relation that $\Phi^i_{11_Z} = \text{R.P.}\ \frac{dW_{11}}{d\sigma}$ and Equation 6, the following integral equation results for $f(\eta)$.

$$\int_0^c \left(\frac{\eta_0}{\eta_0 - \eta}\right) d\eta_0 = 1 + \delta\eta - i\frac{\Gamma}{2\pi}\left(\frac{1}{\eta + i\chi_1} - \frac{1}{\eta - i\chi_i}\right) \equiv H(\eta) \tag{8}$$

The inversion of this equation can be obtained from Reference 17 or 18 as

$$f(\eta) = -\frac{1}{\pi^2}\sqrt{\frac{c-\eta}{\eta}}\int_0^c \sqrt{\frac{\eta_0}{\eta_0 - c}}\,\frac{H(\eta_0)}{\eta_0 - \eta}\,d\eta_0$$

$$= -\frac{1}{\pi}\sqrt{\frac{c-\eta}{\eta}}\left\{1 + \delta\eta + \frac{\delta c}{2}\right\} + i\frac{\Gamma}{2\pi^2}\sqrt{\frac{c-\eta}{\eta}}\left\{\frac{1}{\eta + i\chi_1}\sqrt{\frac{\chi_1}{\chi_1 - ic}} - \frac{1}{\eta - i\chi_1}\sqrt{\frac{\bar{\chi}_1}{\chi_1 + ic}}\right\} \tag{9}$$

The solution to Equation 8 is not unique in that a term of the form $const/\sqrt{\eta(\eta - c)}$ may be added to $f(\eta)$ and still satisfy the equation. This term, however, would introduce undesired singular behavior at the edges of the cavity and therefore has been discarded.

The leading edge Kutta condition or requirement for smooth outflow at the wing edges is

$$\left.\frac{dW_{11}}{dx}\right|_{x=0} = 0 \tag{10}$$

which implies that

$$f(0) = 0$$

or

$$-\left(1 + \frac{\delta c}{2}\right) + \frac{\Gamma}{2\pi}\left\{\frac{1}{\chi_1}\sqrt{\frac{\chi_1}{\chi_1 - ic}} + \frac{1}{\bar{\chi}_1}\sqrt{\frac{\bar{\chi}_1}{\bar{\chi}_1 + ic}}\right\} = 0 \tag{11}$$

In the limit $c \to 0$ this condition reduces to the Kutta condition for the Brown and Michael flow model.

For conical flow the outer boundary of the cavity should be expressible as

$$Y = \bar{e}\,a\,h\,T\left(\frac{Z}{h}\right)$$

Then the requirement that the outer edge of the cavity is a stream surface is that

$$\Phi^i_{11_Y}(0, Z) - (hT)_s = 0$$

Using the conical flow assumptions this may be expressed as

$$hT = z\int_{\lambda}^{z} \phi^{i}_{11_T}(0,z_o)\frac{dz_o}{z_o^2} = \pi z\int_{0}^{\eta} f(\eta_o)\frac{d\eta_o}{h^2-\eta_o^2}$$

Then the requirement for cavity closure is $T = 0$ at $c = 0$

$$\int_0^c \frac{f(\eta_o)}{h^2-\eta_o^2}\,d\eta_o = 0$$

or

$$-\frac{1}{2}\left(1+\frac{\delta c}{2}\right)\left[\sqrt{\frac{h+c}{h}}-\sqrt{\frac{h-c}{h}}\right]-\frac{1}{2\bar{\epsilon}}\left[2-\sqrt{\frac{h+c}{h}}-\sqrt{\frac{h-c}{h}}\right]$$

$$+\frac{i\Gamma}{2\pi}\left\{\sqrt{\frac{\chi_1}{\chi_1-ic}}\left(\frac{1}{h^2+\chi^2}\left[\sqrt{\frac{\chi_1-ic}{\chi_1}}-1\right]-\frac{1}{2h(h+i\chi_1)}\left[\sqrt{\frac{h-c}{h}}-1\right]-\frac{1}{2h(h-i\chi_1)}\left[\sqrt{\frac{h+c}{h}}-1\right]\right)\right. \tag{12}$$

$$\left.-\sqrt{\frac{\bar{\chi}_1}{\bar{\chi}_1-ic}}\left(\frac{1}{h^2+\bar{\chi}_1^2}\left[\sqrt{\frac{\bar{\chi}_1+ic}{\bar{\chi}_1}}-1\right]-\frac{1}{2h(h+i\bar{\chi}_1)}\left[\sqrt{\frac{h-c}{h}}-1\right]-\frac{1}{2h(h-i\bar{\chi}_1)}\left[\sqrt{\frac{h+c}{h}}-1\right]\right)\right\}$$

$$= 0$$

In the limit $c \to 0$ this equation becomes an identity.

The force balance on the concentrated vortex and feeding sheet (cut in complex potential) is given by

$$\Gamma\left[\frac{\bar{\epsilon}}{2}\frac{dW_{11}^{*}}{d\sigma}-\frac{d\bar{\sigma}_1}{ds}\right] = \frac{d\Gamma}{ds}(\bar{\sigma}_1-h) \tag{13}$$

where $\frac{dW_{11}^{*}}{d\sigma}$ is $\frac{dW_{11}}{d\sigma}$ evaluated at σ_1 less the singular contribution from the vortex located at σ_1. For the conical flow Γ and σ_1 scale with h and Equation 13 becomes

$$i\bar{\epsilon}\frac{\sigma_1}{\chi_1}\left\{I-1+\frac{\Gamma}{2\pi h}\frac{1}{\chi_1+\bar{\chi}_1}\right\}+\frac{i\Gamma\bar{\epsilon}}{\pi\sigma_1\chi_1^2}-(2\bar{\sigma}_1-1) = 0 \tag{14}$$

where

$$I = \int_0^c \frac{f(\eta_0)}{\eta_0 + i\chi_1}\, d\eta_0 = \left(1 + \frac{\delta c}{2}\right)\left[1 - \sqrt{\frac{\chi_1 - ic}{\chi_1}}\right] - \delta\left(\frac{c}{2} + i\chi_1\left[1 - \sqrt{\frac{\chi_1 - ic}{\chi_1}}\right]\right)$$

$$- \frac{i\Gamma c}{4\pi} \frac{1}{\chi_1(\chi_1 - ic)} - \frac{\Gamma}{2\pi(\chi_1 + \bar{\chi}_1)} \sqrt{\frac{\bar{\chi}_1}{\bar{\chi}_1 + ic}} \left\{ \sqrt{\frac{\bar{\chi}_1 + ic}{\bar{\chi}_1}} - \sqrt{\frac{\chi_1 - ic}{\chi_1}} \right\}$$

In the limit $c \to 0$ this equation reduces to the corresponding force balance for the Brown and Michael flow model.

Equations 11, 12, and 14 then provide sufficient conditions to determine the unknown parameters c, Γ, and σ_1. This system of equations must be solved numerically. The details of how this was accomplished are given in Appendix B.

Results and Conclusions

The system of equations for the unknown parameter c, Γ and σ is nonlinear and hence the number of roots is unknown. It may be seen by inspection of the equations that Equations 11 and 14 reduce to the corresponding system of equation for the Brown and Michael cross-flow model in the limit $c \to 0$. Also, Equation 12 becomes an identity in this limit. Therefore, the Brown and Michael values for the vortex parameters and $c = 0$ will satisfy the system of equations. This is not the desired solution and will not be discussed further.

The only solutions with nonzero c that have been found are shown in Figures 6, 7, 8, and 9. These roots have physical significance only below $\bar{\epsilon} = 0.206$ and hence the figures are restricted to this range. As seen in Figure 6, above $\bar{\epsilon} = 0.206$, c becomes negative which implies that the cavity shifts to the wing lower surface. This clearly contradicts experimental observations. Furthermore, in the range of $\bar{\epsilon}$ where c is positive, c is very small and the corresponsing vortex parameters are within one half of one percent of the corresponding Brown and Michael values. (Therefore these values have not been included in the figures.) Wing surface pressure distributions for $\bar{\epsilon} = 0.1$ (near the maximum cavity width) are shown in Figure 10 for the Brown and Michael cross-flow model and Figure 11 for the cavity cross-flow model. Although the cavity does not significantly change the vortex position or strength, the upper surface suction peak is slightly reduced, producing a slightly lower normal force coefficient. Although these changes are in the right direction, the magnitude is inconsequential and therefore this specific cavity cross-flow model has little application to the slender wing problem.

The failure of this flow model must be due to either the conical streamline condition imposed upon the cavity or the cavity closure condition. In the present flow model it was assumed that the cavity closed at the wing leading edge. It is possible that the cavity may close inboard of the leading edge (some argument may be made for this assumption by inspection of surface flow studies of Reference 13) or may not close at all. The present experimental observations are insufficient to answer this question conclusively.

A flow model in which it is assumed that the cavity closes inboard of the leading edge contains an additional unknown parameter, namely the location of the outboard edge of the cavity. It appears that such a model could be made determinate by eliminating the singular behavior at the outboard cavity edge, but this flow model has not been investigated in detail.

An alternative condition to replace the conical streamline condition on the cavity might be deduced from that used in Reference 15. The cavity cross-flow model used in Reference 15 for the cavitating low-aspect-ratio hydrofoil problem evidently produces realistic results for that problem. In that analysis a constant pressure boundary condition is imposed on the cavity. The specific form used was that the spanwise velocity component on the cavity was a constant, which is tantamount to assuming that the vorticity in the cavity is constant. This interpretation of the boundary condition used might be plausible for an aerodynamic problem. It is difficult to assess beforehand how this would affect the solution for the model presently used. However, the flow model used in Reference 15 results in singularities at both edges of the cavity. The leading edge singularity may be removed by adding the primary vortex to the flow model, but it is not immediately evident how the singularity at the inboard edge of the cavity may be removed.

There are then several plausible modifications to the present flow model that might be considered but essentially on a trial and error basis. However, there appears to be a more systematic way to address the problem. Thus far the relevant theories have been using potential flow in an attempt to model a flow in which viscosity plays an important role. (The primary and secondary separation are directly attributable to the presence of viscosity.) Any potential flow model which attempts to model these features is inherently indeterminate. The attempts to resolve these indeterminacies have been to deduce the proper boundary conditions by studying experimental observation in which viscosity is inherent. Thus far, however, the proper boundary conditions have not been completely identified. Moreover it appears that the surest way to significant progress on solving these problems would be to consider a flow model in which the viscous terms are present in the equations of motion thus eliminating the need for additional boundary conditions.

VI. SECOND ORDER THEORY FOR CAVITY FLOW MODEL

The previously described cavity flow model has been formally incorporated into the second order theory developed in Reference 6. Recall that

$$\psi_1^o \sim \underline{\eta} + a\,\phi_{11_J}^o + a^2\phi_{11_B}^o \tag{15}$$

$$\psi_1^i \sim a\,\bar{\Phi}_{11}^i + a^3\bar{\Phi}_{121}^i + a^3 \ln a\,\bar{\Phi}_{122}^i \tag{16}$$

where

$$\bar{\Phi}_{11}^i = R.P.\ W_{11} + G_1(s)$$

and W_{11} is given by Equation 6, $\phi_{11_B}^o$ is given by Equation 2, and $\phi_{11_D}^o$ is given by Equation 3. Now, using the asymptotic matching principle and equating the outer expansion of Equation 16 to the inner expansion of Equation 15 results in

$$Q(s) = \int_0^c f(\eta_0)\,d\eta_0 \tag{17}$$

and

$$\bar{P}(s) = 4\pi \frac{d}{ds}\left\{\frac{h^2}{2} + \frac{\Gamma}{2\pi}(\chi_1 + \bar{\chi}_1) - \int_0^c \eta_0 f(\eta_0)\,d\eta_0\right\} \tag{18}$$

$$G_1(s) = Q(s) \ln\left(\frac{4\beta a}{h}\right) \tag{19}$$

Now $\bar{\Phi}_{121}^i$ satisfies the inhomogeneous partial differential equation given by Equation 27 of Reference 6 and boundary condition given by Equation 30 thereof. The method of solution is also the same as that of Reference 6. $\bar{\Phi}_{121}^i$ is composed of a particular part and a homogeneous part and may be expressed as

$$\bar{\Phi}_{121}^i = R.P.\ W_{121}(\sigma) + H_3\,\bar{\Phi}_{11}^i \tag{20}$$

$$W_{121} = -i\frac{\beta^2}{4}\frac{\partial^2}{\partial S^2}\left\{(\bar{\sigma}-\sigma)\left(\frac{\sigma}{2}\sqrt{\sigma^2-h^2}-\frac{h^2}{2}\cosh^{-1}\frac{\sigma}{h}\right)+\frac{\Gamma}{2\pi}(\bar{\sigma}-\sigma)\left(\sigma\ln\left(\frac{\chi-\chi_1}{\chi+\bar{\chi}_1}\right)\right.\right.$$

$$\left.+\sigma_1\ln\frac{2}{h}\left(\frac{\sigma\sigma_1+h^2+\chi_1\chi}{\chi-\chi_1}\right)-\bar{\sigma}_1\ln\frac{2}{h}\left(\frac{\sigma\bar{\sigma}_1-h^2-\chi_1\chi}{\chi-\bar{\chi}_1}\right)-\chi_1\ln\frac{2}{h}(\sigma+\chi)-\bar{\chi}_1\ln\frac{2}{h}(\sigma-\bar{\chi}_1)\right)\Bigg\}$$

$$+\frac{\beta^2}{4}\frac{\partial^2}{\partial S^2}\int_0^c f(\eta_0)\left\{\sigma(\bar{\sigma}-\sigma)\ln(\chi-i\eta_0)-\sigma(\bar{\sigma}-\sigma)+i\eta_0(\bar{\sigma}-\sigma)\ln\frac{2}{h}(\sigma+\chi)\right. \qquad (21)$$

$$\left.-(\bar{\sigma}-\sigma)\sqrt{h^2-\eta_0^2}\ln\frac{2}{h}\left(\frac{\sigma\sqrt{h^2-\eta_0^2}+h^2+i\eta_0\chi}{\chi-i\eta_0}\right)\right\}d\eta_0$$

The unknown portion of the second term of Equation 19 is determined by matching of inner and outer solutions to be

$$H_3(S) = -\beta^2\tilde{P}\left(\frac{1}{4}\ln\frac{16}{\beta}-\frac{1}{4}\right)+\frac{\beta^2}{8}\left[-\frac{1}{2}+\frac{2\Gamma\lambda}{\pi}-\frac{\gamma}{\pi}\left(\frac{P}{2}\ln\frac{(P-\lambda)^2+(\tau-q)^2}{(P+\lambda)^2+(\tau+q)^2}\right.\right.$$

$$\left.\left.+q(\theta_{1_V}+\theta_{2_V})\right)+\ln 2+2(I_3+I_4)\right] \qquad (22)$$

where

$$\tilde{P} = \frac{1}{2}+\frac{\gamma\lambda}{\pi}-I_3$$

$$I_3 = \frac{c^2}{8}-\frac{c^3}{8\bar{\epsilon}}-\frac{\Gamma}{2\pi}\,I.P.\sqrt{\frac{\chi_1}{\chi_1-ic}}+\frac{\Gamma}{\pi}\,R.P.(\chi_1)$$

$$I_4 = \int_0^c \sqrt{h^2-\eta_0^2}\,f(\eta_0)\tan^{-1}\frac{\eta_0}{\sqrt{h^2-\eta_0^2}}\,d\eta_0$$

$$\theta_{1_V} = \tan^{-1}\frac{\tau-q}{P-\lambda} \quad ; -\frac{\pi}{2} < \theta_{1_V} < \frac{\pi}{2}$$

$$\theta_{2_V} = \tan^{-1}\frac{\tau+q}{P+\lambda} \quad ; -\frac{\pi}{2} < \theta_{2_V} < \frac{\pi}{2}$$

The I_4 integral must, in general, be evaluated numerically. The coefficient of the logarithmic term in Equation 16, ϕ'_{122} satisfies LaPlace's equation and may be expressed as

$$\phi'_{122} = H_4(s)\,\phi'_{11} \tag{23}$$

The H_4 function is again determined by matching of inner and outer expansions to be

$$H_4 = \frac{\beta^2}{8\pi}\,\bar{P}(s) \tag{24}$$

To calculate wing surface pressures it is not necessary to determine any more of the higher order solutions (see Reference 6). The inner solution for the straining is, however, required and this is the same as that determined in Reference 6, i.e.,

$$\xi'_1 = -M^2\phi'_{11} + F$$

where F vanishes on the wing.

In Reference 6 the surface pressures were calculated from the velocity potential by using an approximate series expansion form of the isentropic pressure-velocity relationship. This was found to give spurious results at high Mach numbers where the series expansion broke down. In the present work the exact expression was used. Then on the wing surface the isentropic pressure-velocity relationship gives the following expression for the pressure coefficient

$$C_p = \frac{2}{\bar{\gamma}M^2}\left\{\left[1 - \frac{(\bar{\gamma}-1)}{2}M^2\left(2\sin\alpha\cos\alpha\,\psi_{1_S} + \sin^2\alpha\left[\psi_{1_\zeta}^2(1+2M^2\cos\alpha) + \psi_{1_\eta}^2 + \psi_{1_S}^2 - 1\right]\right)\right]^{\frac{\bar{\gamma}}{\bar{\gamma}-1}} - 1\right\} \tag{25}$$

where the quantities in this expression are evaluated on the wing surface and are given by the following expressions.

On the upper surface

$$\psi_{1_S}^2 = (1 + 2a^2H_3 + 2a^2\ln a\,H_4)\,\phi'^2_{11_\Sigma}$$

and

$$\Phi^{i}_{11_{\bar{z}}} = \frac{\bar{z}}{\eta}\left\{-1 - I_1 + \frac{\gamma\lambda}{\pi(\lambda^2+(\eta-\tau)^2)}\right\} \qquad \text{for } 0 \le \bar{z} \le \lambda_c$$

$$= \delta\bar{z} \qquad \text{for } \lambda_c \le \bar{z} \le 1$$

where $\eta = \sqrt{1-\bar{z}^2}$ and $\bar{z}$ is the fraction of half span.

$$I_1 = -\left(1 + \frac{\delta c}{2} + \delta\eta\right)\left(1 - \sqrt{\frac{\eta-c}{\eta}}\right) + \frac{\delta c}{2} + \frac{\gamma}{2\pi}\sqrt{\frac{\eta-c}{\eta}}\, T_2 + \frac{\gamma\lambda}{\pi(\lambda^2+(\eta-\tau)^2)}$$

$$T_2 = \frac{1}{\lambda^2+(\tau-\eta)^2}\left\{2(\eta-\tau)\,I.P.\sqrt{\frac{\chi_1}{\chi_1-ic}} - 2\lambda\, R.P.\sqrt{\frac{\chi_1}{\chi_1-ic}}\right\}$$

$$\psi^2_{1_{\underline{\eta}}} = \left(1 + \delta a^2 H_3 + 2a^2 \ln a H_4\right)\Phi^{i\,2}_{11_\gamma}$$

$$\Phi^{i}_{11_\gamma} = 0 \qquad \text{for } 0 \le \bar{z} \le \lambda_c$$

$$= -\frac{\bar{z}}{\eta}\left\{1 + \frac{\delta c}{2} + \delta\eta + \frac{\gamma}{2\pi}T_2\right\}\sqrt{\frac{c-\eta}{\eta}} \qquad \text{for } \lambda_c \le \bar{z} < 1$$

$$\psi_{1_s} = a\left(1 + a^2 H_3 + a^2 \ln a H_4\right)\Phi^{i}_{11_s}$$

$$\psi^2_{1_s} = a^2\,\Phi^{i\,2}_{11_s}$$

$$\Phi^{i}_{11_s} = G_1 + \frac{1}{2\eta}\left\{1 - \frac{\bar{z}^2\gamma\lambda}{\pi(\lambda^2+(\eta-\tau)^2)} - \bar{z}^2 I_1\right\}$$

$$+ \frac{\gamma}{4\pi}\left(\theta_{1_u} - \theta_{2_u}\right) \qquad \text{for } 0 \le \bar{z} \le \lambda_c$$

$$= G_1 + \frac{1}{2}\left(\eta - \delta\bar{z}^2\right) + \frac{\gamma}{4\pi}\left(\theta_{1_u} - \theta_{2_u}\right) \qquad \text{for } \lambda_c \le \bar{z} < 1$$

where

$$G_1 = \tilde{Q} \ln\left(\frac{4a}{\beta}\right)$$

$$\tilde{Q} = -\frac{c}{2} - \frac{3c^2\delta}{8} + \frac{\gamma}{\pi}\, I.P. \sqrt{\frac{x_1}{x_1 - ic}}$$

$$\theta_{1_u} - \theta_{2_u} = \pi + 2\alpha_1$$

$$\alpha_1 = \tan^{-1}\frac{\tau - \eta}{\lambda} \; ; \qquad -\frac{\pi}{2} < \alpha_1 < \frac{\pi}{2}$$

On the lower wing surface

$$\Phi^{i}_{11_2} = -\frac{z}{\eta}\left\{ I_2 - 1 + \frac{\gamma\lambda}{\pi(\lambda^2 + (\tau+\eta)^2)} \right\} \qquad 0 \le z < 1$$

where

$$I_2 = (\delta\eta - 1 - \frac{\delta c}{2})\left(\sqrt{\frac{\eta + c}{\eta}} - 1\right) + \frac{\delta c}{2} + \frac{\gamma}{2\pi}\sqrt{\frac{\eta+c}{\eta}}\, T_1 - \frac{\gamma\lambda}{\pi(\lambda^2 + (\eta+\tau)^2)}$$

$$T_1 = \frac{1}{\lambda^2 + (\eta+\tau^2)}\left\{ 2(\eta+\tau)\, I.P. \sqrt{\frac{x_1}{x_1 - ic}} + 2\lambda\, R.P. \sqrt{\frac{x_1}{x_1 - ic}} \right\}$$

$$\Phi^{i}_{11_Y} = 0$$

$$\Phi^{i}_{11_S} = G_1 - \frac{1}{2\eta}\left\{ 1 - z^2 - z^2 F_3 \sqrt{\frac{\eta + c}{\eta}} + \delta\eta z^2 \right\} + \frac{\gamma}{4\pi}(\theta_{1_L} - \theta_{2_L})$$

for $0 \le z < 1$

where

$$F_3 = \delta\eta - 1 - \frac{\delta c}{2} + \frac{\gamma}{2\pi} T_1$$

$$\theta_{1_L} - \theta_{2_L} = -\pi - 2\alpha_2$$

$$\alpha_2 = \tan^{-1} \frac{\tau+\eta}{\eta} \; ; \quad -\frac{\pi}{2} < \alpha_2 < \frac{\pi}{2}$$

And at $z = 1$ on the upper surface for $c \neq 0$

$$\bar{\Phi}^i_{11_S} = \frac{\gamma}{4\pi} (\theta_{1_u} - \theta_{2_u}) + G_1 - \frac{\delta}{2}$$

$$\bar{\Phi}^i_{11_Y} = 0$$

$$\bar{\Phi}^i_{11_Z} = \delta$$

On the lower surface if $c \neq 0$

$$\bar{\Phi}^i_{11_S} = \frac{\gamma}{4\pi} (\theta_{1_L} - \theta_{2_L}) + G_1 - \frac{\delta}{2}$$

$$\bar{\Phi}^i_{11_Y} = 0$$

$$\bar{\Phi}^i_{11_Z} = \delta$$

These expressions have been used to calculate the surface pressures for a case in the $\bar{\epsilon}$ range where $c \neq 0$ for the cavity cross-flow model. These results are shown in Figure 11. The limiting forms of the expressions when

c going to zero were also used to calculate the corresponding pressure distribution for the Brown and Michael flow model. These results are shown in Figure 10.

A comparison of the two pressure-velocity relationships is shown in Figure 12. It is seen that the exact isentropic relationship is somewhat better than the approximate form; however, the upper surface suction peak is still overpredicted. The exact expression proves to have a limited range of applicability. At sufficiently high Mach numbers and/or angle of attack the theory predicts surface velocities that exceed those corresponding to vacuum conditions (because the primary vortex is too close to the wing surface). A comparison of the lift predicted by the two forms of the pressure-velocity relationship provides a better estimate of lift in the regions where the calculations can be performed (Figure 1

VII. CONCLUSIONS

A new flow model for the prediction of the flow about delta wings with leading-edge separation was investigated. The flow model included a representation of the secondary separation region that has been experimentally observed on such wings. Secondary separation was modeled as a cavity. The resulting solution for the flow model proves to have only a very limited range (near zero angle of attack) of physical significance. Thus, these results cast suspicion upon the boundary conditions that were used to make the model determinate. These boundary conditions consisted of a cavity closure condition and a requirement for conical streamlines in the cavity region. These assumptions are plausible, based upon the available experimental evidence, but evidently one or both are incorrect. It appears that the correct choice of boundary conditions can be developed only by considering a flow model that retains viscous terms in the equations of motion.

Appendix A

CROSS FLOW MODEL WITHOUT CONCENTRATED VORTICES

As mentioned in Section V of this report a flow model was investigated in which the primary separation was modeled by a surface signularity distribution.

The appropriate complex velocity potential is

$$W_{11} = -iz + \int_0^c f(\eta_0) \ln (z - i\eta_0)\, d\eta_0 \tag{A1}$$

The conical streamline requirement on the cavity gives

$$f(\eta) = -\frac{1}{\pi}\sqrt{\frac{c-\eta}{\eta}}\left[1 + \delta\left(\frac{c}{2} + \eta\right)\right] + \frac{kc}{\sqrt{\eta(c-\eta)}} \tag{A2}$$

With this flow model there must be a singularity at either or both edges of the cavity depending on the specification of k. The choice $k = \frac{1}{\pi}\left(1 + \frac{\delta c}{2}\right)$ meets a Kutta condition at the leading edge and produces a quarter root singularity at λ_c. The resulting slender-wing normal force is then given by

$$C_N = \frac{\pi A}{2} \sin\alpha \left\{1 - \frac{3}{4} c^2 \left(1 + \frac{c}{2\bar{\epsilon}}\right) + \frac{c^2}{8\bar{\epsilon}}\right\} \tag{A3}$$

It is seen from this expression that the cavity produces a non-linear contribution to the lift which is opposite in sign of that of experimental observation.

The choice $k = 0$ produces no singularity at λc, however results in a three-quarter root singularity at the leading edge. (The physical interpretation of this leading edge singularity is questionable.) The corresponding slender-wing normal force coefficient is given by

$$C_N = \frac{\pi A}{2} \sin\alpha \left\{1 + \frac{c^2}{4}\left(1 - \frac{c}{2\bar{\epsilon}}\right) - \frac{c^2}{8\bar{\epsilon}}\right\} \tag{A4}$$

It is possible for the nonlinear contribution to be of the proper sign, and hence further analysis was conducted.

In these flow models c is determined by the requirement for cavity closure. Mathematically this is $\int_0^c \frac{f(\eta_0)}{h^2 - \eta_0^2}\, d\eta_0 = 0$

or

$$-\frac{1}{2}\left(1+\frac{\delta c}{2}\right)\left[\sqrt{\frac{h+c}{h}}-\sqrt{\frac{h-c}{h}}\right]-\frac{1}{2\bar{\epsilon}}\left[2-\sqrt{\frac{h+c}{h}}-\sqrt{\frac{h-c}{h}}\right]=0 \qquad \text{(A5)}$$

This equation only has solutions for $\bar{\epsilon} > 23.3$ This large an $\bar{\epsilon}$ value is well out of the ranges of practical value.

Hence it was concluded that cross flow models of this type were of no use for the slender wing problem.

Appendix B

NUMERICAL SOLUTION OF THE CROSS-FLOW EQUATIONS

The system of equations to be solved for the unknown parameters c, Γ, σ_1 is composed of Equation 11, 12, and 14. The basic method employed was a Newton-Raphson iteration scheme. First, the equations are normalized by dividing all lengths by h and by letting $\gamma = \Gamma/h$. Then γ is eleiminated from the system by using Equation 11, viz.

$$\gamma = \frac{\pi\left(1 + \frac{\delta c}{2}\right)}{R.P\left\{\frac{1}{\chi_1}\sqrt{\frac{\chi_1}{\chi_1 - ic}}\right\}} \tag{B1}$$

and the following functions are defined.

$$CF12 = \frac{i\chi_1}{\sigma_1 \bar{\epsilon}}(2\bar{\sigma}_1 - 1) + \frac{\gamma}{\sigma_1^2 \chi_1 \pi} + I - 1 + \frac{\gamma}{2\pi}\frac{1}{\chi_1 + \bar{\chi}_2} \tag{B2}$$

and

$$F1 = R.P.\ CF12 \tag{B3}$$

$$F2 = I.P.\ CF12 \tag{B4}$$

From Equation 7

$$F'3 = \left(1 + \frac{\delta c}{2}\right)\left(\sqrt{1+c} - \sqrt{1-c}\right) - \frac{1}{2\bar{\epsilon}}\left(2 - \sqrt{1+c} - \sqrt{1-c}\right)$$

$$+ \frac{\gamma}{\pi} I.P.\left\{\sqrt{\frac{\chi_1}{\chi_1 - ic}}\left(\frac{1}{1+\chi_1^2}\left[\sqrt{\frac{\chi_1 - ic}{\chi_1}} - 1\right] - \frac{1}{2(1 - i\chi_1)}\left[\sqrt{1-c} - 1\right]\right.\right. \tag{B5}$$

$$\left.\left. - \frac{1}{2(1 + i\chi_1)}\left[\sqrt{1+c} - 1\right]\right\}\right.$$

and

$$F3 = F'3/c^2 \tag{B6}$$

The values of χ_1 and c which simultaneously zero the F_i functions are then the desired solution to the problem. The Newton procedure is outlined below.

An initial guess at the solution at a selected $\bar{\epsilon}$ value is made, say, $\chi(1)$ and $c(1)$. Further let $X_1 = R.P.\,\chi_{(1)}$, $X_2 = I.P.\,\chi_{(1)}$ and $X_{(3)} = c$. Then it is assumed that if these guesses are close to the solution that

$$F_i \approx F_i(1) + \Delta X_i \left.\frac{\partial F_i}{\partial X_i}\right|_{X_i(1)} \qquad i = 1,2,3 \qquad \text{(B7)}$$

then the increments in the variables to reach the solution are found by solving the linear system of equations.

$$\Delta X_i \frac{\partial F_i}{\partial X_i} = -F_i(1) \qquad i = 1,2,3 \qquad \text{(B8)}$$

or

$$\Delta X_1 = \frac{1}{D}\begin{vmatrix} -F1(1) & \frac{\partial F1}{\partial X_2} & \frac{\partial F1}{\partial X_3} \\ -F2(1) & \frac{\partial F2}{\partial X_2} & \frac{\partial F2}{\partial X_3} \\ -F3(1) & \frac{\partial F3}{\partial X_2} & \frac{\partial F3}{\partial X_3} \end{vmatrix}$$

where

$$D = \begin{vmatrix} \frac{\partial F1}{\partial X_1} & \frac{\partial F1}{\partial X_2} & \frac{\partial F1}{\partial X_3} \\ \frac{\partial F2}{\partial X_1} & \frac{\partial F2}{\partial X_2} & \frac{\partial F2}{\partial X_3} \\ \frac{\partial F3}{\partial X_1} & \frac{\partial F3}{\partial X_2} & \frac{\partial F3}{\partial X_3} \end{vmatrix}$$

All the partial derivatives are evaluated at $X_i(1)$. There are similar expressions for ΔX_2 and ΔX_3. The next guess at the solution is then $X_i(2) = X_i(1) + \Delta X_i(1)$. This process is then repeated until all $|F_i(n)| < 10^{-6}$. The partial derivatives of the F_i were computed using the finite difference approximation. The initial difference was chosen as $.01 X_i$. The difference for the successive steps where chosen as the $\Delta X_i(n-1)$ at each step.

This scheme was programmed for the Calspan/IBM 370 computing machine. The resulting solutions for non-zero c and vortex positions are shown in Figures 6, 7, 8, and 9.

Initially the system was used with F'3 as given by Equation B5. This system of equations (with the method of solution used) would only converge to

solutions for which $C \neq 0$. Analysis of Equation B5 for small c then showed that $F3$ vanished as c^2 for small c, hence $F3$ was formed and this system resulted in the solutions shown.

The entire system of equations was analyzed for small c because it was intuitively thought that there should be a solution with c small, at least in the lower $\bar{\epsilon}$ range. This analysis showed some properties of the system of equations that were interesting in their own right and therefore this analysis is outlined below.

Equations 11, 12, and 14 were expanded for small c. The results are as follows. The leading edge Kutta condition, Equation 11, becomes

$$F_{1_{BM}} + cf_1 + \frac{3}{16} c^2 f_2 + o(c^3) = 0 \tag{B9}$$

where

$$F_{1_{BM}} = -1 + \frac{\gamma}{2\pi}\left(\frac{1}{\chi_1} - \frac{1}{\bar{\chi}_1}\right)$$

$$f_1 = -\frac{1}{2\bar{\epsilon}} + \frac{i\gamma}{4\pi}\left(\frac{1}{\chi_1^2} - \frac{1}{\bar{\chi}_1^2}\right)$$

$$f_2 = -\frac{\gamma}{\pi}\left(\frac{1}{\chi_1^3} + \frac{1}{\bar{\chi}_1^3}\right)$$

The closure condition, Equation 12, becomes

$$\frac{c}{2} F_{1_{BM}} + \frac{3}{4} c^2 f_1 + c^3\left(\frac{1}{16} F_{1_{BM}} + \frac{5}{32} f_2\right) + o(c^4) = 0 \tag{B10}$$

The force balance on the primary vortex and feeding sheet, Equation 14, becomes

$$F_{3_{BM}} + cf_3 + c^2 f_4 + o(c^3) = 0 \tag{B11}$$

where

$$F_{3_{BM}} = -\frac{1}{2}(2\bar{\sigma}_1 - 1) + \frac{\bar{\epsilon} i}{2}\left\{\frac{\gamma}{2\pi}\frac{1}{\chi_1 + \bar{\chi}_1} - 1\right\}\frac{\sigma_1}{\chi_1} + \frac{i\gamma\bar{\epsilon}}{2\pi}\frac{1}{\sigma_1 \chi_1^2}$$

$$f_3 = i\left\{\frac{1}{2\chi_1} - \frac{\gamma}{4\pi\chi_1^2} + \frac{\gamma}{4\pi}\frac{1}{\chi_1+\bar{\chi}_1}\left(\frac{1}{\chi_1}+\frac{1}{\bar{\chi}_1}\right)\right\}$$

$$f_4 = \frac{i}{4\bar{\epsilon}\chi_1} - \frac{1}{8\chi_1^2}\left(1 - i\frac{\chi_1}{\bar{\epsilon}}\right) + \frac{\gamma}{4\pi}\frac{1}{\chi_1^3}$$

$$- \frac{\sigma}{2\pi}\frac{1}{\chi_1+\bar{\chi}_1}\left\{\frac{1}{8}\left(\frac{1}{\chi_1^2}-\frac{1}{\bar{\chi}_1^2}\right) + \frac{i}{4\chi_1}\left(\frac{1}{\chi_1}+\frac{1}{\bar{\chi}_1}\right)\right\}$$

Now it is recognized that $F_{1_{BM}} = 0$ and $F_{3_{BM}} = 0$ are respectively the leading edge Kutta condition and the force balance on primary vortex and its feeding sheet for the Brown and Michael cross-flow model. Hence, as $c \to 0$ Equation B10 vanishes as c^2. This explains why the original system of equations would only converge to solutions with $c = 0$.

Furthermore $c/2$ may be factored out of Equation B10 resulting in

$$F_{1_{BM}} + \frac{3}{2}cf_1 + c^2\left(\frac{1}{8}F_{1_{BM}} + \frac{5}{16}f_2\right) + o(c^3) = 0 \qquad \text{(B12)}$$

Then Equation B9, B11 and B12 form the approximate equation for the cross-flow model for small c.

Comparison of the approximate closure condition, Equation B12 and the approximate Kutta condition, Equation B9 shows that to zeroth order in that these conditions are not independent. Because of the special form of Equations B9 and B12 they may be combined to give

$$c = \frac{f_1}{5f_2 + \frac{5}{16}F_{1_{BM}}} \qquad \text{(B13)}$$

so that c may be eliminated from the system of equations. Then Equation B9 and B11 constitute a sufficient system to determine γ and χ_1. This approximate system must also be solved numerically and this was done in a fashion similar to the full equations. The solutions to the approximate system were found to **have the same general behavior as the solutions to the full system and thus reinforced the results previously given for the full system.**

REFERENCES

1. Polhamus, E.C.: Predictions of Vortex Lift Characteristics Based on a Leading Edge Suction Analogy. AIAA Paper No. 69-1133, Oct. 1969.

2. Brown, C.E.; and Michael, W.H., Jr.: On Slender Delta Wings with Leading-Edge Separation. NACA TN 3430, Apr. 1955.

3. Mangler, K.W.; and Smith, J.H.B.: Calculations of the Flow Past Slender Delta Wings with Leading Edge Separation. R.A.E. Report Aero 2593, May 1957.

4. Smith, J.H.B.: Improved Calculations of Leading-Edge Separation from Slender Delta Wings. R.A.E. Technical Report No. 66070, Mar. 1966.

5. Mangler, K.W.; and Weber, J.: The Flow Field Near the Center of a Rolled-Up Vortex Sheet. Journal of Fluid Mechanics, vol. 30, part I, 1967, pp. 177-196.

6. Nenni, J.P.; and Tung, C.: A Second Order Slender Wing Theory for Wings with Leading Edge Separation in Supersonic Flow. NASA-CR-1860 Sept. 1971.

7. McGregor, I.: Development of the Vapor Screen Method of Flow Visualization in a 3 Ft. x 3 Ft. Supersonic Wind Tunnel. Part IV of Flow Visualization in Wind Tunnels Using Indicators, compiled by R.L. Maltby, AGARDograph 70, Apr. 1962.

8. Burgesen, A.J.; and Porter, J.D.: An Investigation of the Flow Around Slender Delta Wings with Leading-Edge Separation. Princeton University Aero-Eng. Dept., Report No. 510, May 1960.

9. Thomann, H.: Measurements of Heat Transfer, Recovery Temperature, and Pressure Distribution on Delta Wings at M = 3. Aeronautical Research Institute of Sweden, FFA Report 93, 1963.

10. Michael, W.H., Jr.: Flow Studies on Flat-Plate Delta Wings at Supersonic Speeds. NACA TN 3472, July 1955.

11. Wickens, R.H.: The Vortex Wake and Aerodynamic Load Distribution of Slender Rectangular Plates, The Effects of a 20-Degree Bend at Mid-Chord. National Research Council of Canada Aeronautical, Report No. LR-458, May 1966.

12. Lemaire, D.A.: Some Observations of the Low-Speed Flow Over a Sharp-Edged Delta Wing of Unit Aspect Ratio. Department of Supply Australian Scientific Service Aeronautical Research Laboratories Aerodynamics, Report 126, Jan. 1965.

13. Squire, L.C.; Maltby, R.L.; Keating, R.F.A.; and Stanbrock, A.: The Surface Oil Flow Technique. Part I of Flow Visualization in Wind Tunnels Using Indicators, compiled by R.L. Maltby, AGARDograph 70, Apr. 1962.

14. Stahl, W.; Hartmann, K.; and Schneider, W.: Force and Pressure Measurements on a Slender Delta Wing at Transonic Speeds and Varying Reynolds Numbers. AGARD Conference Pre-Print No. 83 on Facilities and Techniques for Aerodynamic Testing at Transonic Speeds and High Reynolds Number, Apr. 1971.

15. Kaplan, P.; Goodman, T.R.; and Chen, C.C.: A Hydrodynamic Theory for Cavitating Delta Wing Hydrofoils. Oceanics, Inc., Technical Report No. 67-33, Dec. 1966.

16. Maskell, E.C.: Flow Separation in Three Dimension. R.A.E., Report No. Aero 2565, Nov. 1955.

17. Carrier, G.F; Krock, M.; and Pearson, C.E.: Functions of a Complex Variable. McGraw-Hill Book Co., 1966.

18. Cheng, H.K; and Rott, N.: Generalizations of the Inversion Formula of Thin Airfoil Theory. Journal of Rational Mechanism and Analysis, vol. 3, no. 3, May 1954.

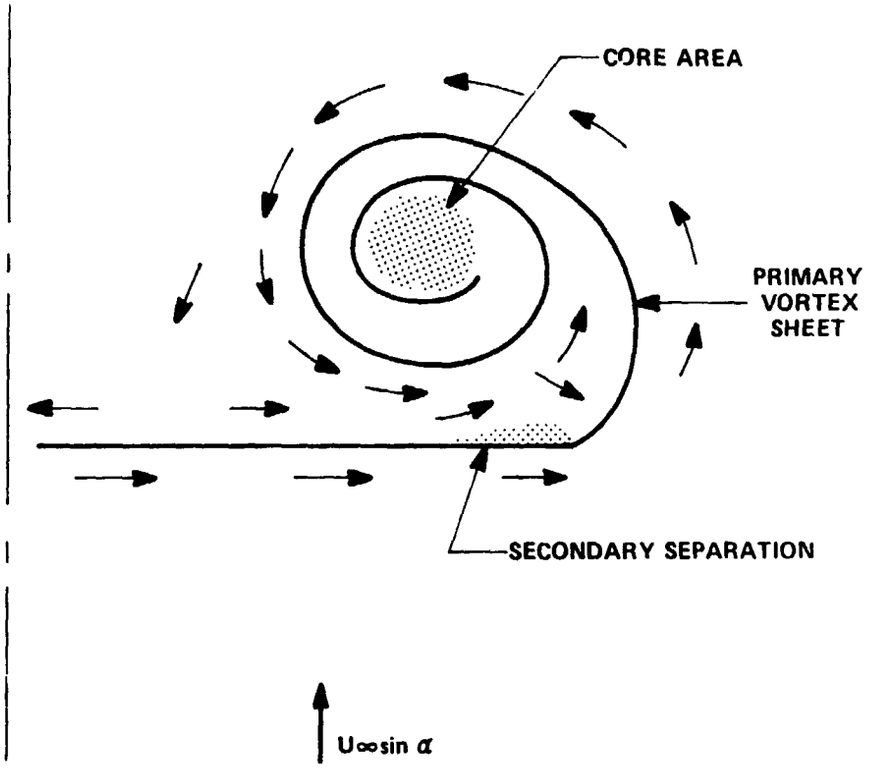

Figure 1 OBSERVED CROSS FLOW (SHADED AREAS INDICATE REGIONS OF SIGNIFICANT TOTAL HEAD LOSS)

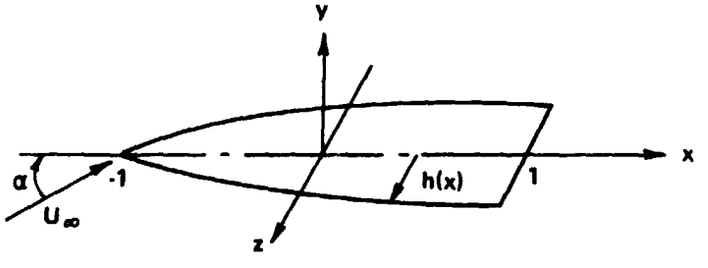

Figure 2 COORDINATE SYSTEM AND WING GEOMETRY

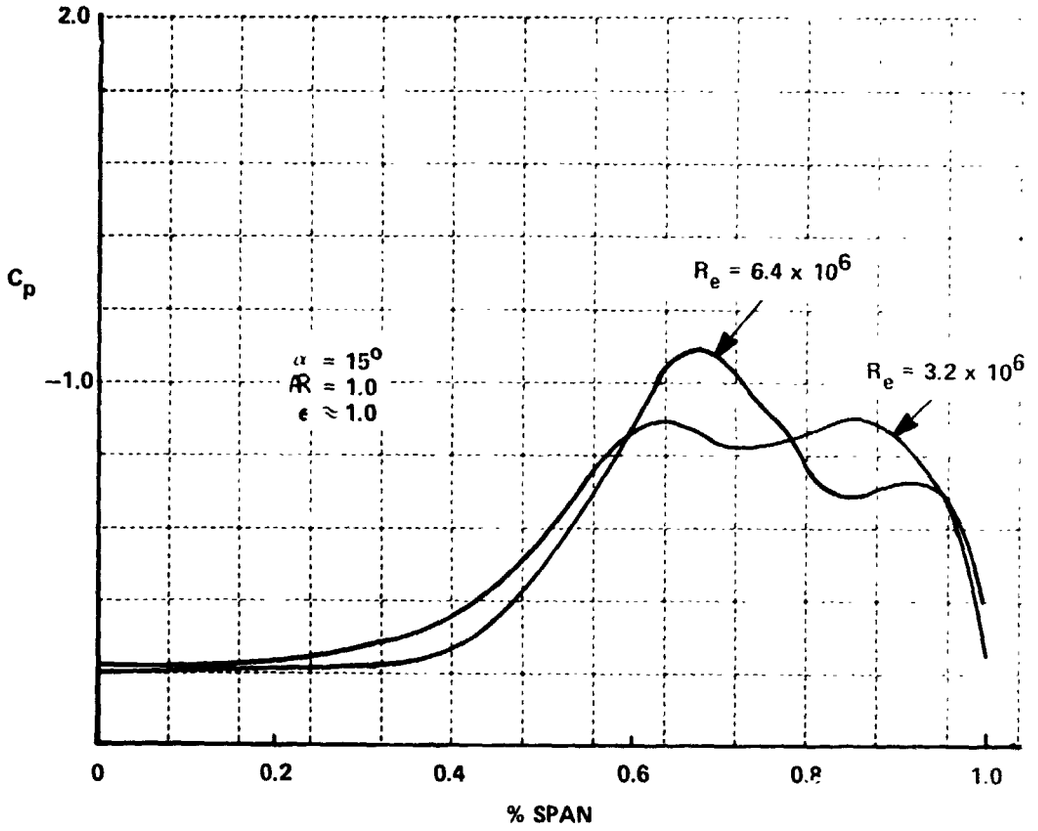

Figure 3 EFFECT OF REYNOLDS NUMBER ON UPPER SURFACE PRESSURE DISTRIBUTION FROM REF. 13

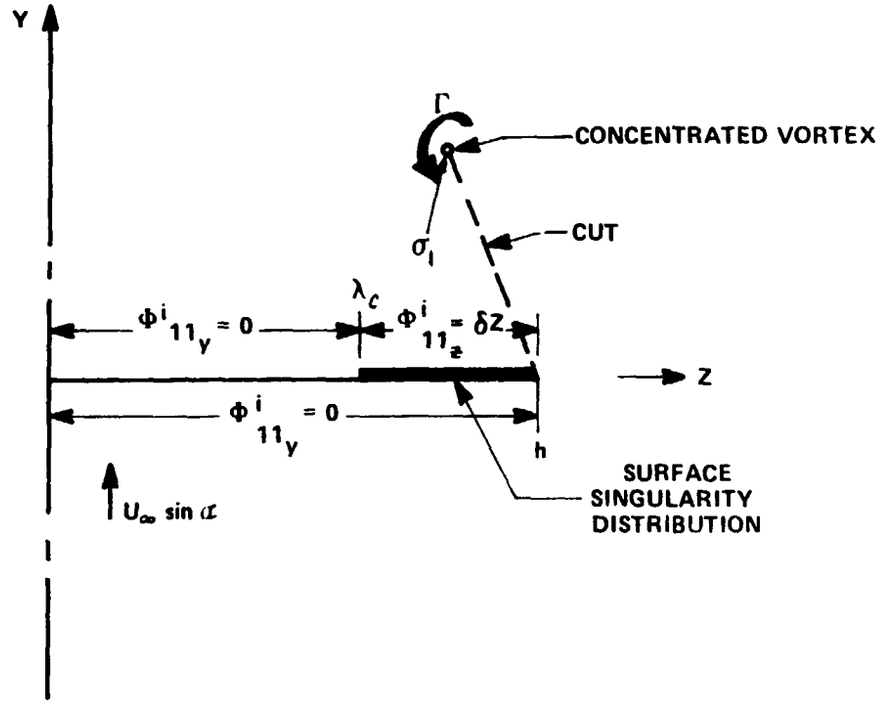

Figure 4 CROSS FLOW MODEL WITH CAVITY IN σ PLANE

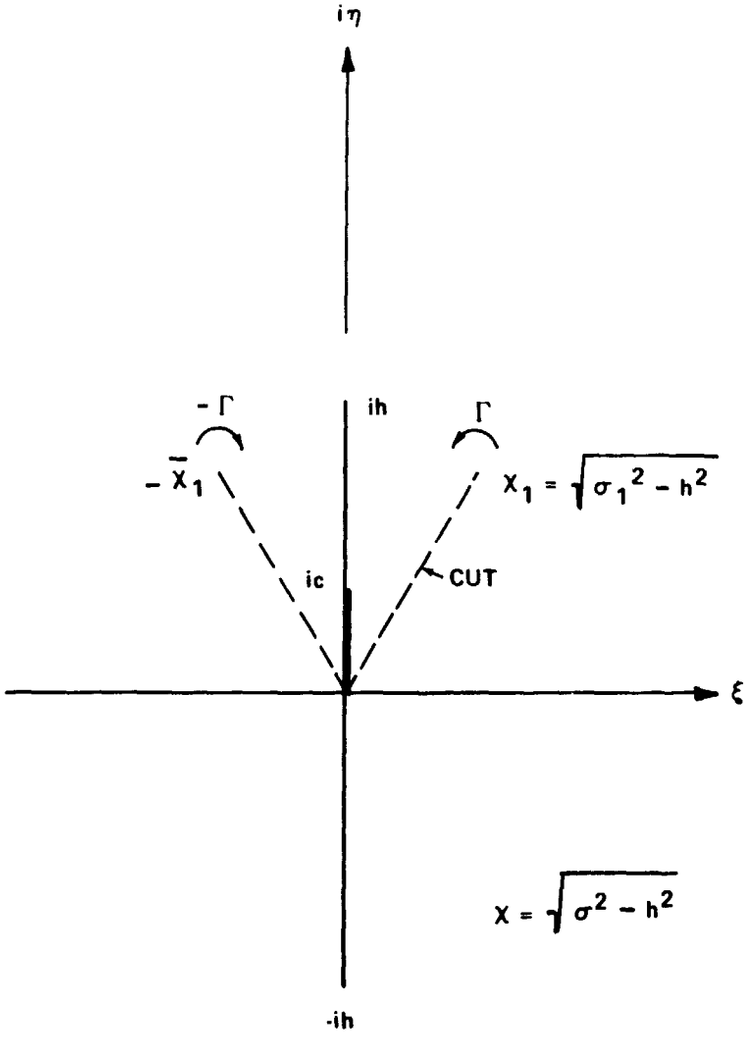

Figure 5 χ PLANE

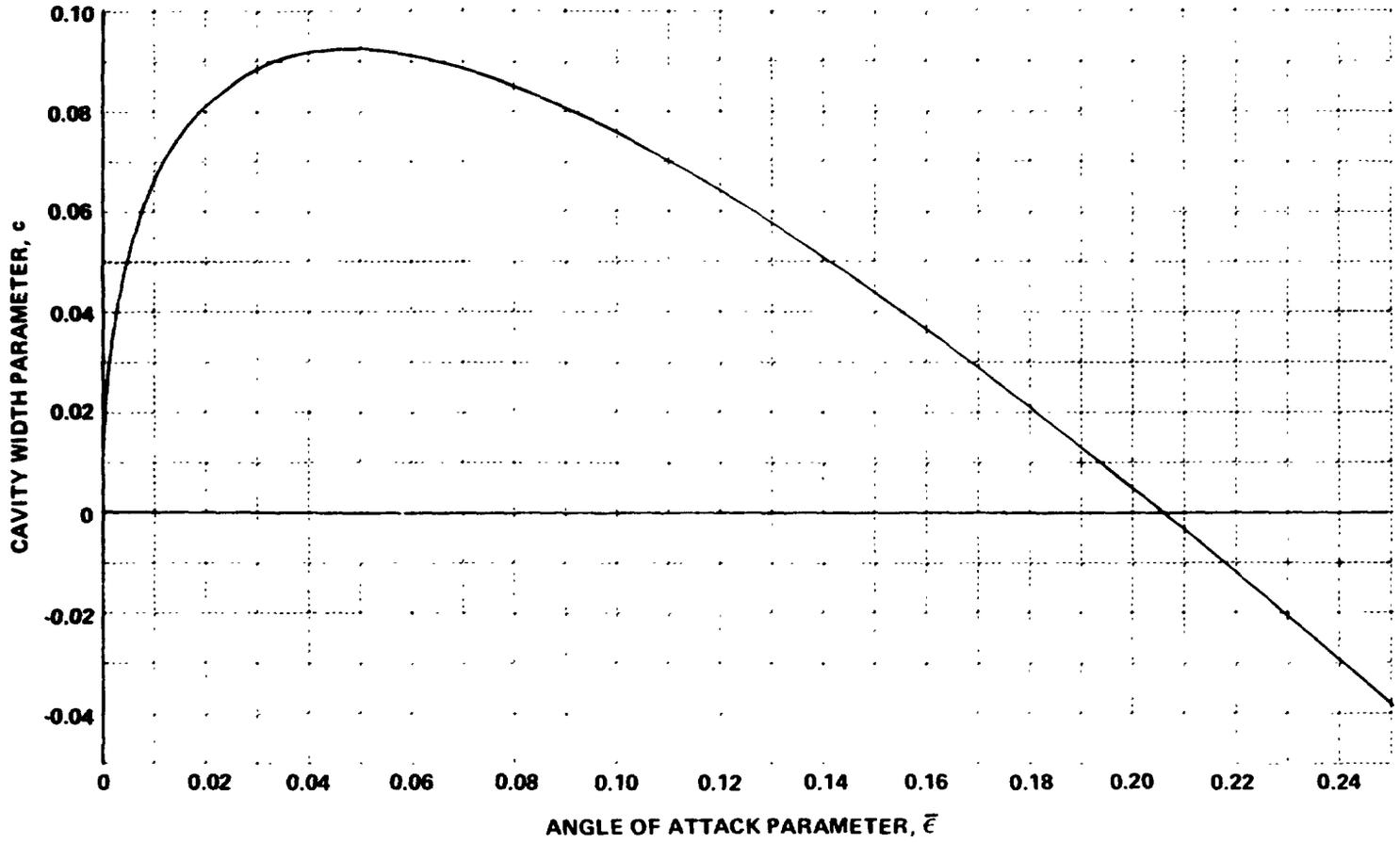

Figure 6 VARIATION OF CAVITY WIDTH PARAMETER WITH ANGLE OF ATTACK PARAMETER

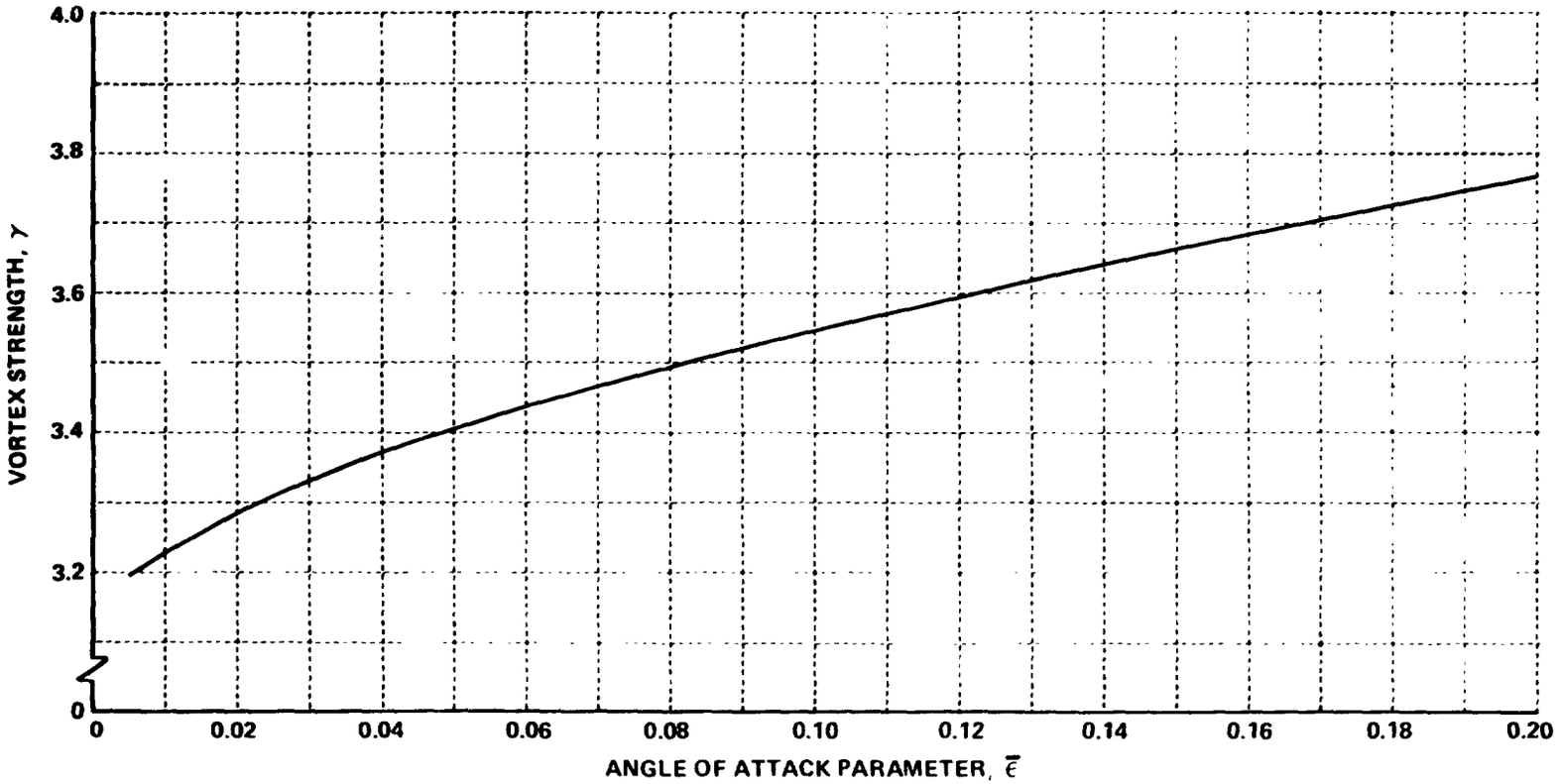

Figure 7 VARIATION OF VORTEX STRENGTH WITH ANGLE OF ATTACK PARAMETER

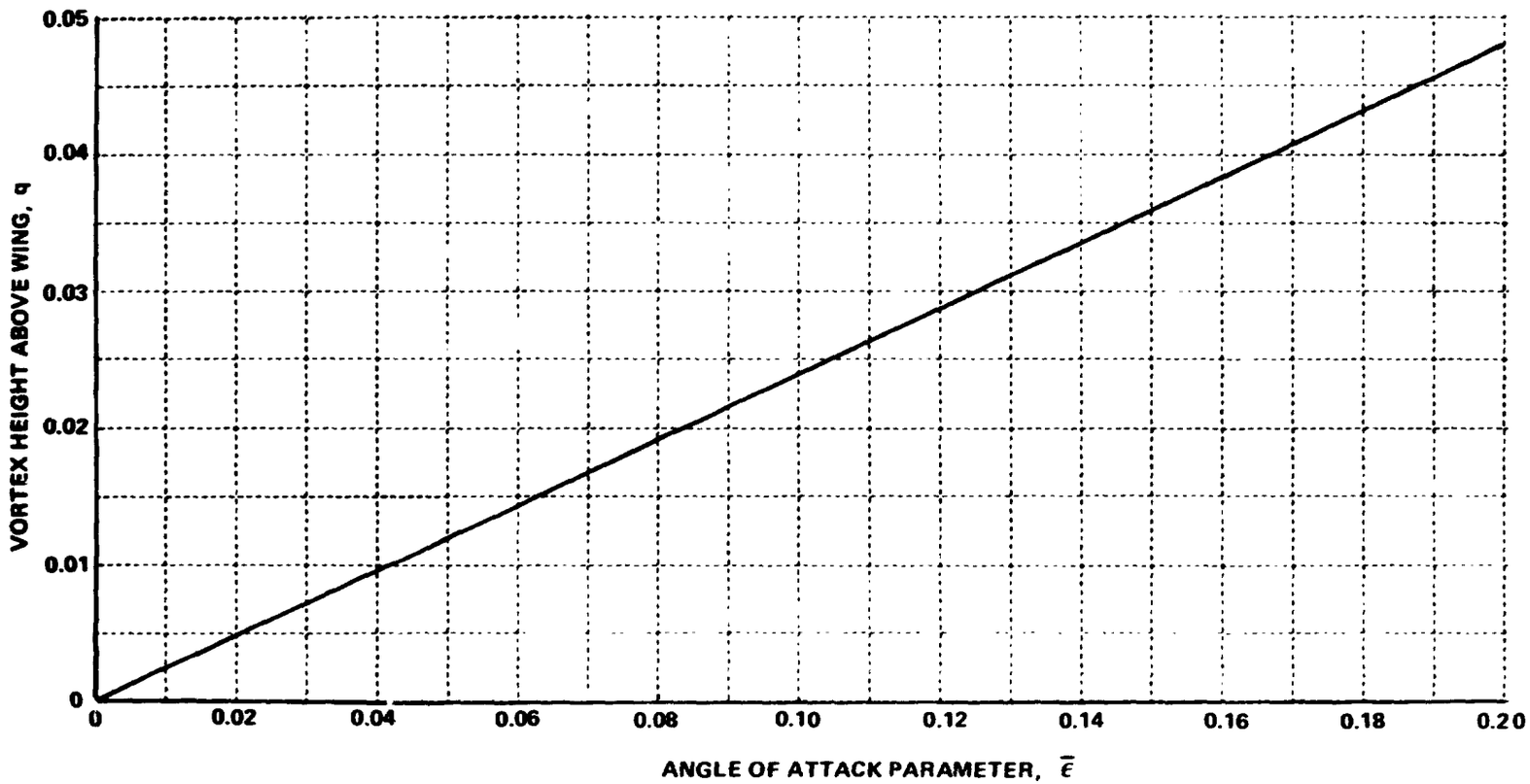

Figure 8 VARIATION OF VORTEX HEIGHT ABOVE WING ANGLE OF ATTACK PARAMETER

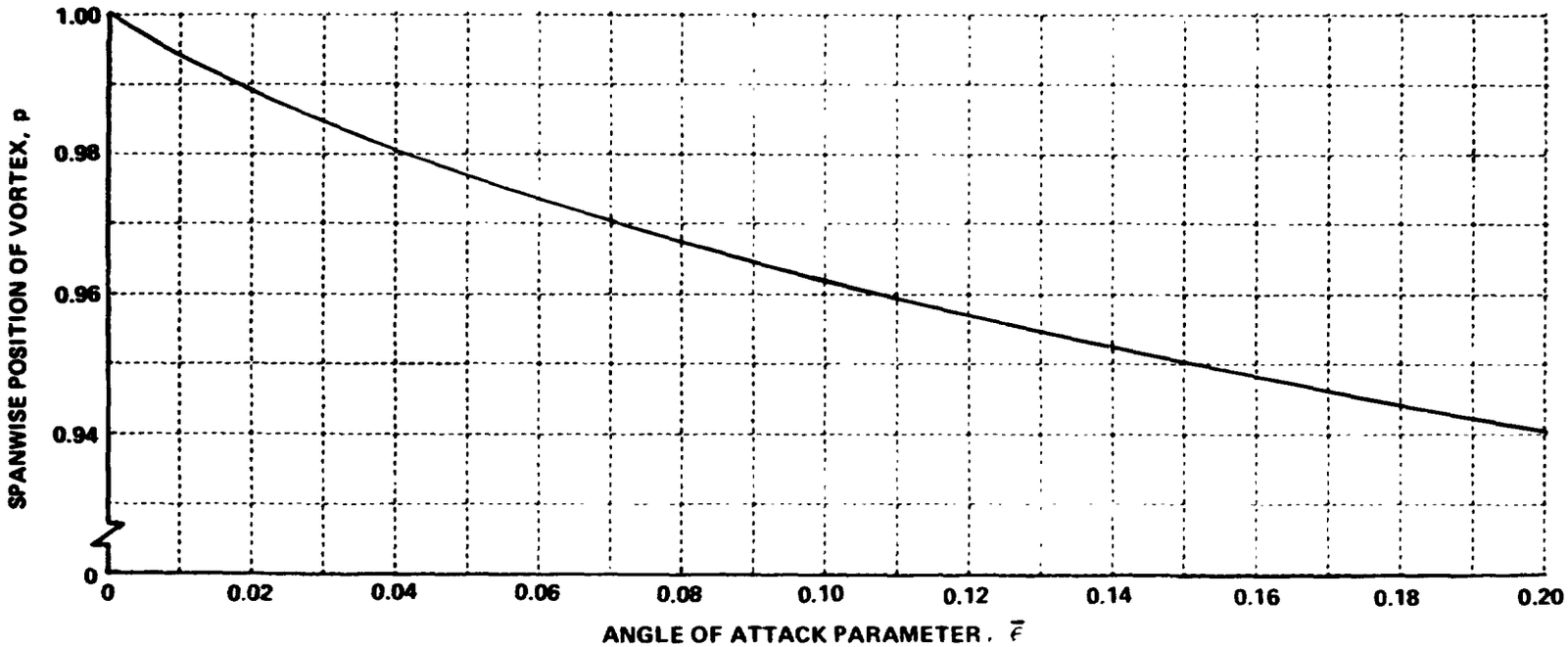

Figure 9 VARIATION OF SPANWISE POSITION WITH ANGLE OF ATTACK PARAMETER

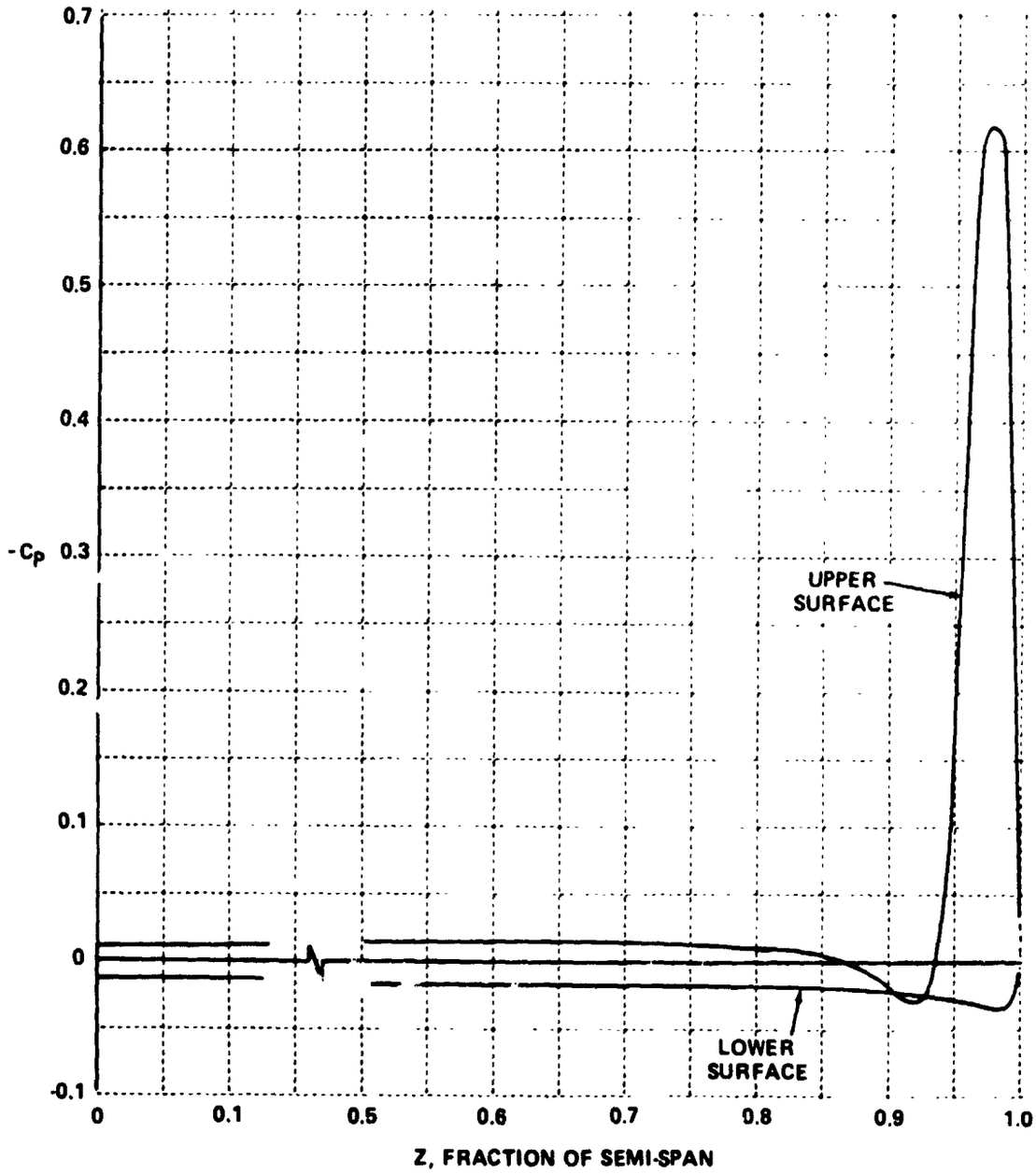

Figure 10 WING SURFACE PRESSURE DISTRIBUTION SECOND-ORDER THEORY WITH BROWN AND MICHAEL CROSS-FLOW MODEL, M = 1.5, $\mathcal{R}$ = 1.0, $\bar{\epsilon}$ = 0.1 (α = 1.43°), C_N = 0.0503

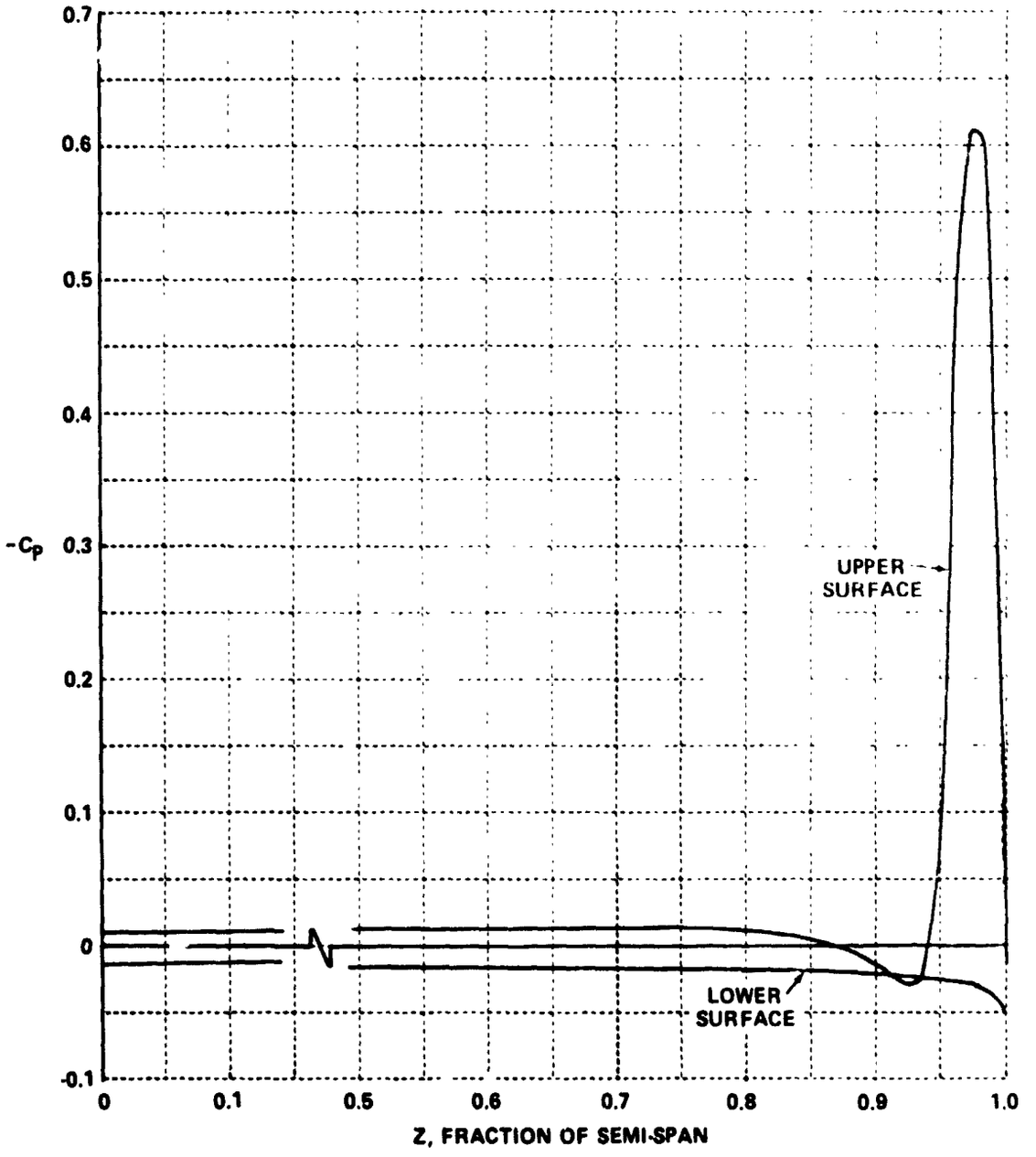

Figure 11 WING SURFACE PRESSURE DISTRIBUTION SECOND-ORDER THEORY CAVITY CROSS-FLOW MODEL, M = 1.5, AR = 1.0, ϵ = 0.1 (α = 1.43°), λ_c = 0.9971, C_N = 0.0485

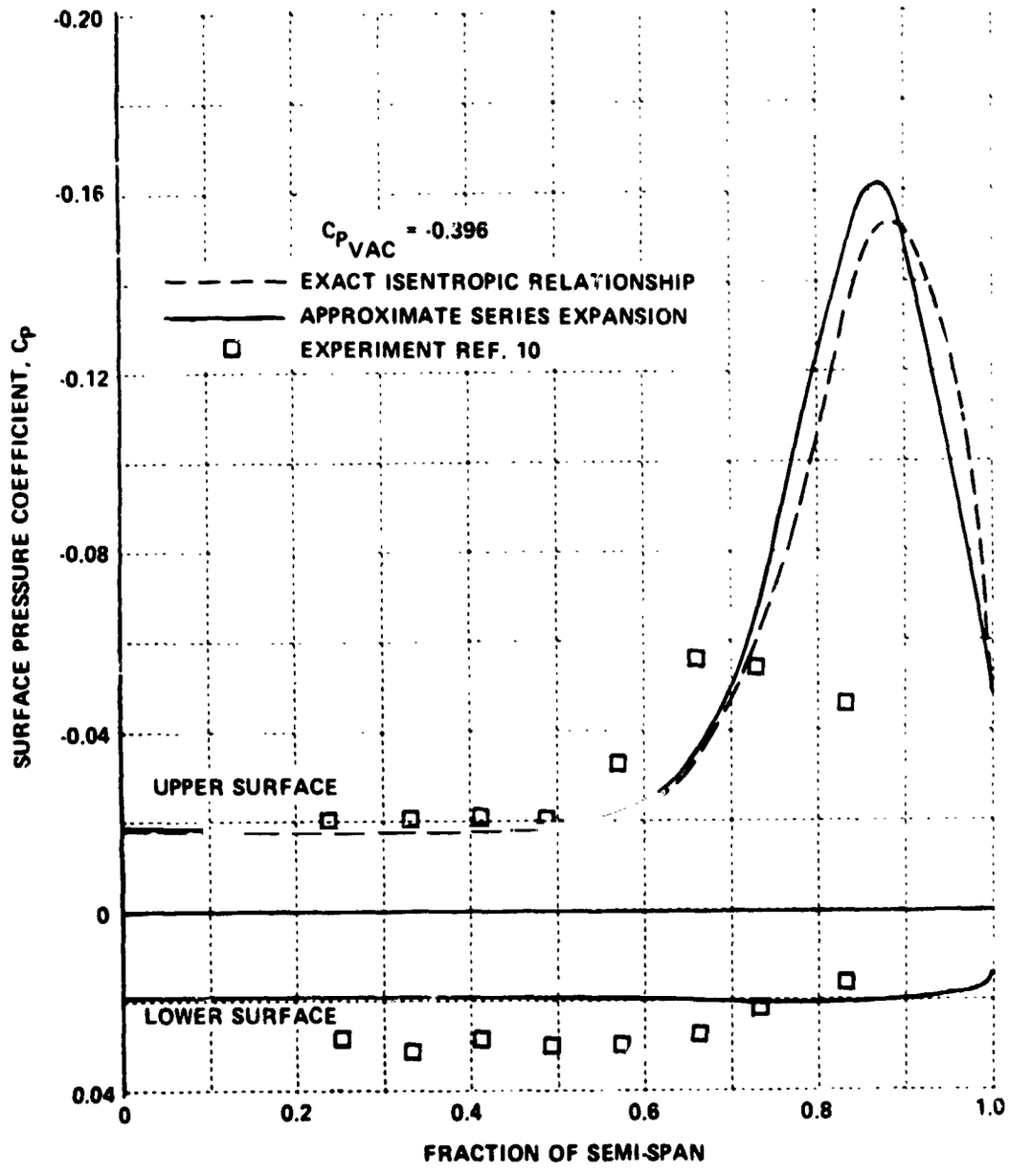

Figure 12 COMPARISON OF SURFACE PRESSURE COEFFICIENT FOR A DELTA WING ($\mathcal{R}$ = 0.35, M = 1.9, $\bar{\epsilon}$ = 0.8 (α = 4°)

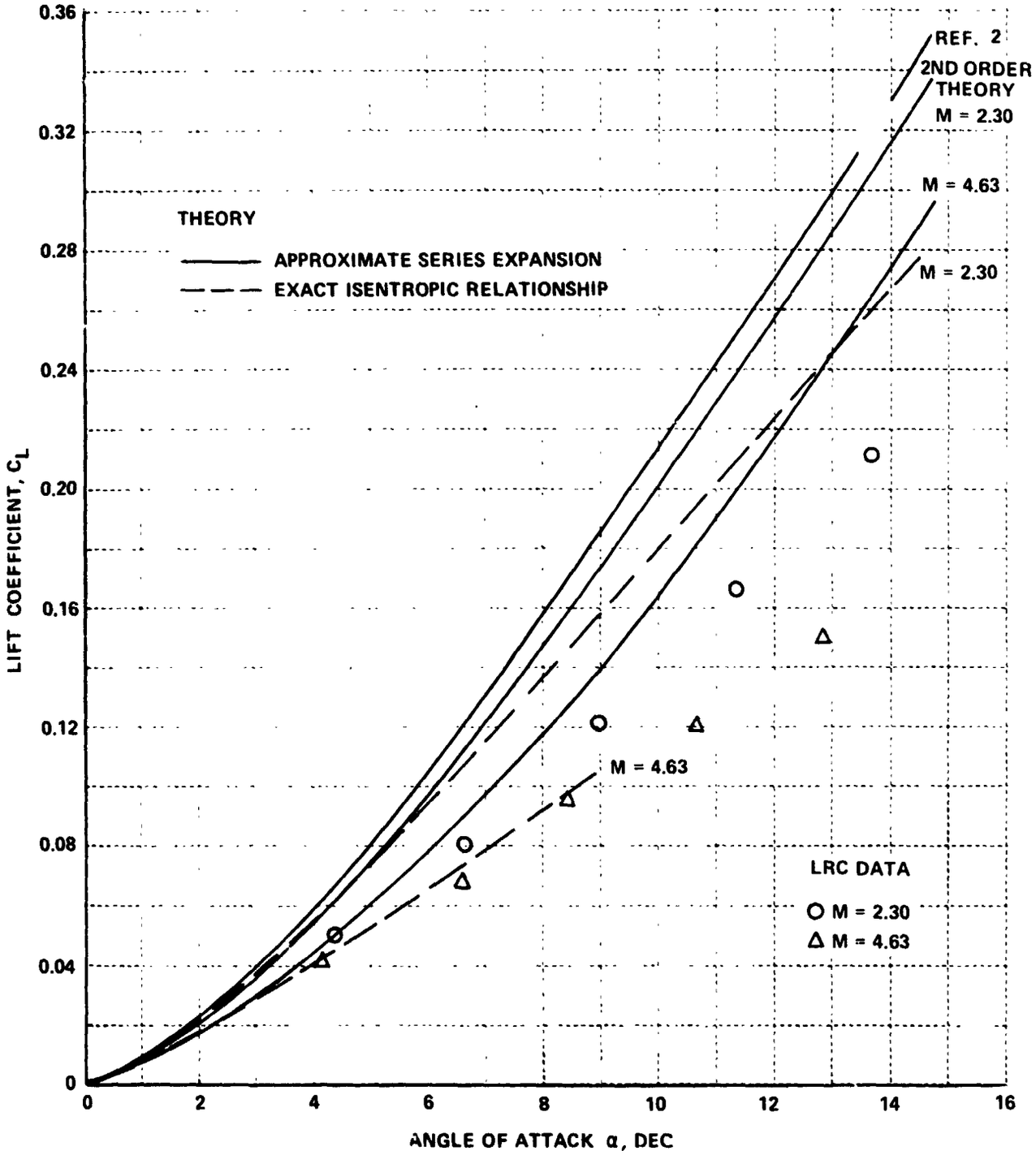

Figure 13 COMPARISON OF THEORETICAL LIFT COEFFICIENTS USING EXACT AND APPROXIMATE ISENTROPIC PRESSURE-VELOCITY RELATIONSHIP $\mathcal{R}$ = 0.25